Special Feature: Design of High-power Lithium-ion Batteries with Long Operational Life

Research Report

Electrochemical Behavior of $LiNiO_2$-derivatives and Their Cycling Stability in the Cylindrical Lithium-ion Batteries

Yoshinari Makimura, Tsuyoshi Sasaki and Takamasa Nonaka

Report received on Aug. 9, 2017

ABSTRACT In lithium-ion batteries, the selection of positive and negative electrode materials enables us to design basic function of the batteries in terms of operating voltage and its shape, and such materials-selection is one of advantages of the lithium-ion technology. Of these, the maximum energy density and cycling stability of lithium-ion batteries are determined by basic characteristics of positive electrode materials. In this paper, materials research on a positive electrode for lithium-ion batteries is highlighted in terms of the formation of solid solution, cation-doping, and ion-exchanging, and recent advances in $LiNiO_2$-relatives are described herein since $LiNiO_2$-relatives exhibit higher rechargeable capacity than others. Factors affecting the cycling life of cylindrical lithium-ion batteries of $LiNi_{0.8}Co_{0.15}Al_{0.05}O_2$ (NCA) with graphite were examined in terms of rechargeable capacity and polarization of NCA-derivatives of $Li_zNi_{0.8}Co_{0.15}Al_{0.05}O_{2-\delta}$ ($0.8 \leq z \leq 1.05$) or of $[Li_{1-y}Ni_y]^{3(b)}[Ni,Co,Al]^{3(a)}O_2{}^{6(c)}$ based on a space group of $R\bar{3}m$ Rechargeable capacities (Q) of the NCA-derivatives examined in sandwich-type lithium cells decrease linearly as the amount of rock-salt domains (y) increases, and an empirical relation told us that Q reaches zero at y = 0.25, which is derived from not only the capacity-loss owing to inactive rock-salt domain but the polarization-increase. Galvanostatic Intermittent Titration Technique (GITT) measurement told us that polarizations of NCA-derivatives increase when the amount of rock-salt domains is above 2%, i.e., $y > 0.02$, and such a relation is remarkable in the lithium insertion direction into the structure, which is ascribed to slow lithium-ion mobility owing to nickel ions in the lithium layers. The extended cycling test for cylindrical lithium-ion batteries of NCA-derivatives with graphite negative-electrode at elevated temperature told us that materials innovation to prevent the formation of rock-salt domains will be an effective way to improve the cycling life of the lithium-ion batteries at elevated temperature.

KEYWORDS Lithium Nickel Oxides, Solid Solution, Layered Material, Positive Electrode, Lithium Battery

1. Introduction

Lithium-ion batteries, in which $LiCoO_2$ and carbon are used as positive and negative electrodes, respectively, were first commercialized in 1991. One of advantages of the lithium-ion battery system is that the batteries can be designed in terms of the operating voltage and its shape by combining two electrode materials at will.[1-4] The electrode material of higher operating voltage is used as a positive electrode and that of lower voltage is a negative electrode. During charge, electrons are extracted from a positive electrode and injected into a negative electrode upon storing electrical energy. At the same time, lithium ions are extracted from/inserted into a solid matrix without the destruction of core structures to compensate an excess charge, namely topotactic reaction. During discharge, the electrochemical reaction takes place in a reverse direction in the battery upon delivering electrical energy. Lithium ions move back and forth between two electrode materials during operation. This is why the batteries were named the lithium-ion "shuttlecock" or "rocking-chair" system in the early stage of battery research. Lithium-ion batteries, which were designed as power sources for portable devices such as mobile phones and notebook computers, have been applied to large-sized energy-storage devices for automotive and stationary purposes.

In lithium-ion batteries, positive electrode materials have been extensively and intensively studied to improve electrochemical reactivity and structural stability since the maximum energy density and cycling

stability of lithium-ion batteries are determined by basic characteristics of positive electrode materials.[1-4] A positive electrode material of $LiCoO_2$ having a layered structure was proposed by Goodenough's group to exhibit reversible charge and discharge behavior in sandwich-type lithium cells.[5] Since $LiCoO_2$ can be materialized easily and exhibits flat operating voltage at about 4 V, $LiCoO_2$ has been used as a positive electrode for small-sized lithium-ion batteries. For large-sized applications, positive electrode materials of manganese, iron, and/or nickel-species have to be used rather than $LiCoO_2$ to lower risk of a resource crisis. Of these, $LiNiO_2$-based materials are attractive because of large rechargeable capacity more than 150 mAh g^{-1}, moderately high operating-voltage above 3.6 V vs. Li, and characteristic S-shaped curve over the entire range of operation.[6,7] In this paper, the research background and recent trends of positive electrode materials having a layered structure are highlighted. Factors affecting the cycling life of cylindrical lithium-ion batteries of $LiNi_{0.8}Co_{0.15}Al_{0.05}O_2$ (NCA) with graphite are discussed in terms of rechargeable capacity and polarization.

1. 1 Structural Description of Lithium Transition Metal Oxides

Figure 1(a) shows lithium transition metal oxides having α-$NaFeO_2$-type layered structure based on a space group of $R\bar{3}m$. $LiMO_2$ (M = V, Cr, Fe, Co, Ni, etc.) are materialized with respect to this structural type in which Li and M ions are located at 3(b) and 3(a) sites, respectively, based on a space group of $R\bar{3}m$. The triangular basal net formed in the octahedral sites is homogeneously occupied by Li or M ions in α-$NaFeO_2$-type structure, which can be described as the [1×1] structure. The basal planes of [1×1] Li and [1×1] M ions are piled up alternately, which gives the composition ratio 1/1 of Li/M to be $LiMO_2$. Analytical data for the crystal structures of layered lithium transition metal oxides are listed in **Table 1**.

Spinel-related lithium transition metal oxides of LiM_2O_4 in which Li ions are located at tetrahedral sites and M ions are at octahedral sites in a cubic close-packed oxygen array based on a space group of $Fd\bar{3}m$ (cubic) or $I4_1/amd$ (tetragonal), e.g., $LiMn_2O_4$ and $Li[Li_{1/3}Ti_{5/3}]O_4$ as listed in Table 1. Spinel-framework structure, in which lithium ions at the tetrahedral sites are ignored, can be described as a layered structure in terms of the basal planes of octahedral sites as shown in Fig. 1(b). In two types of basal planes, vacant (□) and M-occupied octahedral sites are arranged regularly to be [2×2] superlattice, which gives the composition of 1/3 (or 3/1) of □/M. The two types of [2×2] superlattice sheets shown in Fig. 1(b) are piled up alternately, giving the one-to-one composition of □- and M-occupied sites to form $□MO_2$. (111) sheets of spinel-framework structure in a cubic lattice can be converted to (003) sheets of α-$NaFeO_2$-type structure

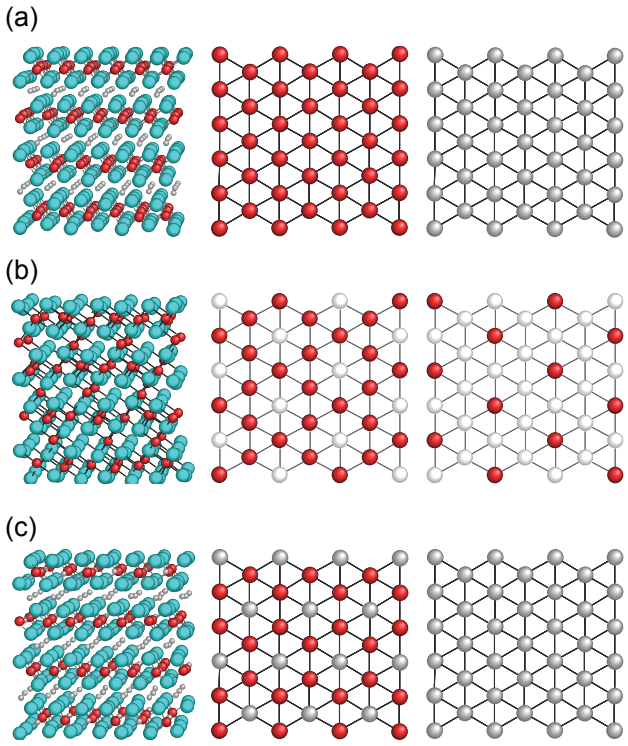

Fig. 1 Schematic illustrations of crystal structure for (a) α-$NaFeO_2$-type structure, (b) spinel-framework structure given in a layered formulation, and (c) Li_2MnO_3; (a) The triangular basal net formed in the octahedral sites is occupied by lithium or transition metal ions; (b) [2×2] superlattice sheets of vacant and occupied octahedral sites by transition metals in ratios of 1 to 3 and 3 to 1 are piled up alternately to form a spinel-framework structure; (c) [√3×√3]R30º superlattice is formed by regular distribution of lithium and manganese ions in a ratio of 1 to 2 in transition metal sheets. Li_2MnO_3 is usually described as $Li[Li_{1/3}Mn_{2/3}]O_2$ in a layered formulation. Large blue spheres indicate oxide ions. Red and gray spheres indicate transition metal and lithium ions, respectively. White spheres displayed in (b) indicate vacant sites. Structural data on corresponding materials are given in Table 1.

by lowering the symmetry. The unit cell of the [2×2] structure is 2 times larger than that of the [1×1] structure. Spinel-framework structure can be described as 25% regular displacement between Li and M ions in two basal planes of α-$NaFeO_2$-type structure.

The crystal structure of Li_2MnO_3 is shown in Fig. 1(c), which can be illustrated as a layered structure. A transition metal sheet is also displayed in this figure. Li and Mn ions are regularly distributed in transition metal sheets to form [√3×√3]R30º superlattice, which gives the composition of 1/2 of Li/M to form [$Li_{1/3}Mn_{2/3}$]. The unit cell is √3 times larger than that of the [1×1] structure with 30º rotation. Layered structure of Li_2MnO_3 is constructed by stacking Li and [$Li_{1/3}Mn_{2/3}$] sheets alternately, and therefore Li_2MnO_3 is described in a layered formulation of Li[$Li_{1/3}Mn_{2/3}$]O_2. As listed in Table 1, a space group symmetry of Li_2MnO_3 has been reported to be *C*2/*m*, but the way to pile up [$Li_{1/3}Mn_{2/3}$] sheets is not unique.[8] **Figure 2** displays possible models stacking [$Li_{1/3}Mn_{2/3}$] sheets to construct the layered structure. In a structural model shown in Fig. 2(a), [$Li_{1/3}Mn_{2/3}$] sheets are piled up straightly in which identical metal ions are aligned in a straight line along c-axis which gives a space group of *C*2/*m*. Figure 2(b) displays the way to stack [$Li_{1/3}Mn_{2/3}$] sheets rotationally corresponding to a space group symmetry of $P3_112$. Figure 2(c) shows another stacking method of [$Li_{1/3}Mn_{2/3}$] sheets in which identical metal ions draw zigzag lines which corresponds to a space group of *C*2/*c*.

Lithium transition metal oxides shown above have cubic-close(st) packed (CCP) oxygen array, which is called O3-stacking with respect to the location of Li ions and the stacking order of MO_2-layers. In these structures, Li ions are surrounded by six oxide ions forming octahedral-type location. A hexagonally closest packing (HCP) is called O1-stacking with respect to the same criteria. These criteria were formulated by Delmas and Hagenmuller's research group.[9] **Figure 3** displays three types of locations of alkali metal ions in which "prismatic", "octahedral", and "tetrahedral" are abbreviated as "P", "O", and "T", respectively. **Figure 4** displays P2 and O2 structure. Sodium transition metal oxides of $Na_{2/3}[M'_xM''_{1-x}]O_2$, in which M' and M'' are Li^+, Mg^{2+}, Ni^{2+}, Co^{3+}, or Mn^{4+}, etc., have been reported to be crystallized as P2 structure.[10] Lithium-based materials obtained by ion exchanging from sodium-based materials having P2 structure convert to O2 and/or T2 structures with stacking fault.[11] These layered materials having unique stacking order have been prepared by well-controlled ion-exchange techniques and proposed that some of these materials exhibit improved electrochemical behavior in sandwich-type lithium cells in comparison to positive electrode materials having O3 stacking.

Table 1 Lithium (or sodium) transition metal oxides reported so far.

Space group	Materials	Lattice parameters	Positions
$R\bar{3}m$	$LiVO_2$*	*a* = 2.836 Å, *c* = 14.767 Å	Li^+ (0, 0, 1/2) M^{3+} (0, 0, 0) O^{2-} (0, 0, 0.26)
	$LiCrO_2$*	*a* = 2.897 Å, *c* = 14.495 Å	
	$LiCoO_2$*	*a* = 2.814 Å, *c* = 14.044 Å	
	$LiNiO_2$*	*a* = 2.880 Å, *c* = 14.187 Å	
*C*2/*m*	$LiMnO_2$	*a* = 5.439 Å, b = 2.809 Å *c* = 5.388 Å, β = 116.01º	Li^+ (0, 1/2, 1/2), M^{3+} (0, 0, 0) O^{2-} (0.27, 0, 0.77)
$Fd\bar{3}m$	Li[$Li_{1/3}Ti_{5/3}$]O_4	*a* = 8.365 Å	Li^+ (1/8, 1/8, 1/8), M^{3+}&M^{4+} (1/2, 1/2, 1/2)
	$LiMn_2O_4$	*a* = 8.240 Å	O^{2-} (0.26, 0.26, 0.26)
*C*2/*m*	Li_2MnO_3	*a* = 4.926 Å, b = 8.531 Å *c* = 9.621 Å, β = 99.76º	Li^+ (0, 1/2, 0) (0, 0, 1/2) (0, 0.661, 1/2) Mn^{4+} (0, 0.167, 0) O^{2-} (0.219, 0, 0.227) (0.254, 0.321, 0.223)
$P6_3/mmc$	P2-$Na_{2/3}CoO_2$	*a* = 2.830 Å, *c* = 10.924 Å	Na^+ (0, 0, 1/4) (2/3, 1/3, 1/4) M^{3+} (0, 0, 0), O^{2-} (1/3, 2/3, 0.077)
$P6_3mc$	O2-$LiCoO_2$	*a* = 2.802 Å, *c* = 9.537 Å	Li^+ (2/3, 1/3, 1/4), M^{3+} (2/3, 1/3, 0) O^{2-} (0, 0, 0.407) (1/3, 2/3, 0.093)

* Lattice parameters are given in a hexagonal setting.

1. 2 Layered Positive Electrode Materials

Among positive electrode materials for lithium-ion batteries, $LiCoO_2$ is well-known and has been widely applied to small-sized lithium-ion batteries for mobile applications. Regarding large rechargeable capacity, natural abundance, and less-toxicity compared with $LiCoO_2$, $LiNiO_2$ has been studied as a possible candidate to replace $LiCoO_2$. $LiNiO_2$ can store and deliver more than 150 mAh g^{-1} of capacity, while the operating voltage is lower than that of $LiCoO_2$.[6] The charge-end voltage of $LiNiO_2$, however, has to be limited below 4.15 V vs. Li because nickel dioxide formed above 4.20 V vs. Li on charge or "over-"charge causes materials degradation and exothermic reaction with nonaqueous electrolyte at elevated temperature around 150ºC due to structural instability. In order to cope with these problems, materials modification has been performed by many research groups.

$LiCoO_2$ is iso-structural with $LiNiO_2$, and both materials consist of a low-spin state of trivalent transition metal ions of Co^{3+} and Ni^{3+} ions. Therefore, a solid solution between $LiCoO_2$ and $LiNiO_2$ is formed as $LiNi_{1-x}Co_xO_2$ ($0 < x < 1$) in which cobalt ions are substituted for nickel ions in $LiNiO_2$, i.e., a substitutional solid solution.[12] When the upper-voltage limit is set above 4.2 V, $LiCoO_2$ and $LiNiO_2$ deteriorate upon cycling. Sandwich-type lithium cells of $LiNi_{1-x}Co_xO_2$ ($0 < x < 1$) can be operated in the charge-end voltage above 4.2 V, and exhibit stable charge and discharge cycling, which is one of the effects of the formation of solid solution. The operating voltage of $LiNi_{1-x}Co_xO_2$ ($0 < x \leq 0.5$) is close to that of $LiNiO_2$. The solid-state redox reaction in $LiNi_{1-x}Co_xO_2$ ($0 < x \leq 0.5$) is associated with nickel species in an early stage of the electrochemical reaction.[13]

Since α-$LiAlO_2$ is also iso-structural with $LiNiO_2$, a solid solution between α-$LiAlO_2$ and $LiNiO_2$ can be formed as $LiNi_{1-x}Al_xO_2$ ($0 < x \leq 1/2$). In $Li_{1-y}NiO_2$, nickel dioxide is formed in the composition range of $3/4 < y \leq 1$ during charge or "over-"charge, inactive metal ions with regard to electrochemical reaction such as aluminum ions are effective to prevent the formation of nickel dioxide. $LiNi_{3/4}Al_{1/4}O_2$ is oxidized up to the

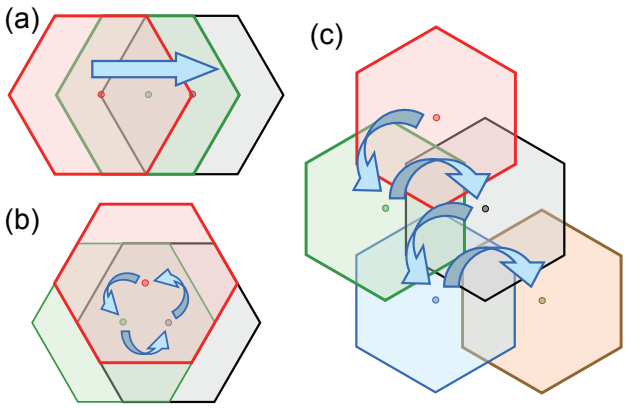

Fig. 2 Schematic illustrations of ways to pile up transition metal sheets depicted as a hexagonal shape to construct layered structures; (a) straight model giving a space group of $C2/m$, (b) screw model giving a space group of $P3_112$, and (c) zigzag model giving a space group symmetry of $C2/c$.

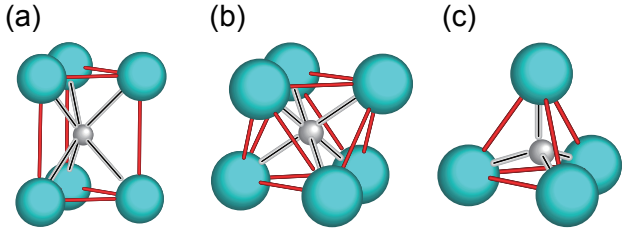

Fig. 3 Three types of locations of alkali metal ions to formulate the crystal structure based on the way to stack MO_2 sheets; (a) "prismatic", (b) "octahedral", and (c) "tetrahedral" locations, which are abbreviated as "P", "O", and "T", respectively. Small gray and large blue spheres indicate alkali metal and oxide ions, respectively.

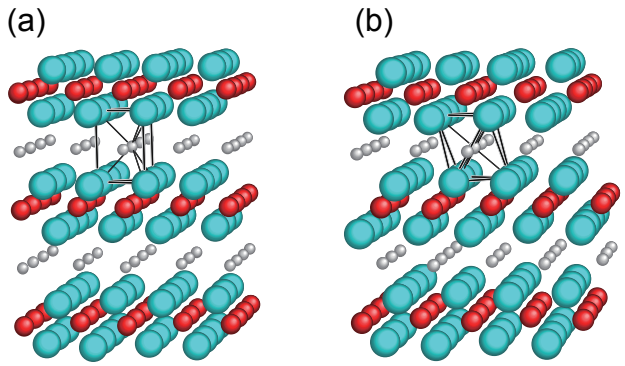

Fig. 4 Schematic illustrations of the crystal structures of (a) $Na_{2/3}[M'_xM''_{1-x}]O_2$ (M' and M'' = Li^+, Mg^{2+}, Ni^{2+}, Co^{3+}, or Mn^{4+}, etc.) having P2 structure, and (b) $Li_{2/3}[M'_xM''_{1-x}]O_2$ having O2 structure obtained by ion exchanging. Large blue spheres indicate oxide ions. Red and gray spheres indicate transition metal and lithium ions, respectively. Structural data on corresponding materials are given in Table 1.

composition of $Li_{1/4}Ni_{3/4}Al_{1/4}O_2$ in sandwich-type lithium cells, which indicates that aluminum ions can protect against the formation of nickel dioxide.[14] Substitution of aluminum ions in $LiNiO_2$ to form $LiNi_{1-x}Al_xO_2$ ($0 < x \leq 1/2$) causes improved capacity retention for a charge-end voltage of more than 4.2 V, increased electrode potentials compared with $LiNiO_2$, and increased safety characteristics to prevent exothermic reactions with electrolyte.

The substitution of metal ions for nickel in $LiNiO_2$ improves the electrochemical reactivity and structural stability of $LiNiO_2$, leading to further materials innovation. Among possible metal ions, cobalt and aluminum ions can be substituted for nickel ions and the obtained $LiNiO_2$-derivatives such as $LiNi_{1-x}Co_xO_2$ and $LiNi_{1-x}Al_xO_2$ based on the formation of solid solution among $LiNiO_2$, $LiCoO_2$, and α-$LiAlO_2$ exhibit superior electrochemical behavior to that of $LiNiO_2$. The co-substitution of Co and Al ions for Ni ions in $LiNiO_2$ was proposed as a promising positive electrode material of $LiNi_{0.8}Co_{0.15}Al_{0.05}O_2$ (NCA) for large-sized lithium-ion batteries.

1. 3 Cycling Stability of Lithium-ion Batteries

Required performances of lithium-ion batteries for large-sized applications are quite challenging for researchers and engineers with respect to durability and safety, and hence operating conditions for lithium-ion batteries have to be monitored and be strictly controlled in terms of temperature, voltage, and current to overcome these concerns.[15-20] Deterioration of lithium-ion batteries by extended cycling or storage tests especially at elevated temperature has been reported by many research groups, which attribute it to degradation of the positive electrode materials such as NCA at a microscopic or macroscopic scale.[19-30] Degradation of the NCA-based positive electrode has been examined with respect to the increase in interfacial resistance at the positive electrode,[21,25] generated micro-cracks in the particles,[19,20] or formation of NiO-like rock-salt domains.[19,20,23,24,30] Similarity of reaction products between exothermic reactions of positive electrode materials at high temperature above 150˚C and materials degradation during cycling at 60˚C strongly suggests that positive electrode materials are a key for tough and safe batteries.[31-34] Our group has reported the deterioration of lithium-ion batteries of NCA with graphite during extended cycling for more than 500 cycles at elevated temperature above 60˚C is derived from the localized degradation of NCA to form NiO-like rock-salt domains in the structure.[28,29] Electrochemical impedance spectroscopy (EIS) measurement of 500 mAh-class cylindrical lithium-ion batteries of NCA with graphite revealed that the rise in internal resistance of the batteries was dominated by the rise in the charge-transfer resistance of the positive electrode, which corresponds to right semicircle resistance in the lower frequency range in the Nyquist plots of two semicircles.[27] Temperature dependence of the charge-transfer resistance of NCA before and after cycling test indicated that the impedance rise of the NCA positive electrode was caused by a reduction in the number of active sites for the charge-transfer process, and hence NiO-like rock-salt domains localized at the surface of the NCA particles were considered to be inactive to reduce the number of active sites.[37] Electrochemical reactivity of the rock-salt domains is actually not obvious and the relation between the formation of rock-salt domains and the deterioration of lithium-ion batteries has not been quantitatively understood because only trace amounts of the rock-salt domains are generated after extended cycling at elevated temperature. In the next sections, NCA-derivatives of $Li_zNi_{0.8}Co_{0.15}Al_{0.05}O_{2-\delta}$ ($0.8 \leq z \leq 1.05$) having quantitatively-controlled rock-salt domains in the structure were prepared and their electrochemical measurements were performed to clarify the relationship between rock-salt domains and electrochemical reactivity in terms of rechargeable capacity and polarization. Extended cycling test of 500 mAh-class cylindrical lithium-ion batteries of NCA-derivatives was also performed, and a possible way to improve battery performance is discussed in the later sections.

2. Experimental

A co-precipitation method was applied to prepare $Li_zNi_{0.8}Co_{0.15}Al_{0.05}O_{2-\delta}$ samples. A mixed solution of nickel, cobalt, and aluminum nitrates and an aqueous solution of lithium hydroxide were dripped simultaneously into a stirred flask. The reaction product to be a precipitate was washed several times with distilled water, and dried at 80˚C for 12 hours. The obtained powder of nickel, cobalt, and aluminum species was mixed with lithium carbonate, and the

reaction mixture was heated at 750˚C under an oxygen stream. The amount of z in $Li_zNi_{0.8}Co_{0.15}Al_{0.05}O_{2-\delta}$ was adjusted by the molar ratios of lithium to nickel, cobalt, and aluminum ions in the starting materials.

The obtained samples of $Li_zNi_{0.8}Co_{0.15}Al_{0.05}O_{2-\delta}$ were characterized by powder X-ray diffraction using a RINT-TTR II powder diffractometer (Rigaku Corp., Japan) with Cu-Kα radiation, and a Rietveld method using the GSAS package with the EXPGUI interface[36] based on the structural model of $[Li_{1-y}Ni_y]^{3(b)}[Ni,Co,Al]^{3(a)}O_2{}^{6(c)}$ assuming a space group of $R\bar{3}m$.

The X-ray absorption spectral measurements of $Li_zNi_{0.8}Co_{0.15}Al_{0.05}O_{2-\delta}$ were carried out at a BL33XU beam-line in SPring-8. A Si(111) channel-cut crystal monochromator was used for incident X-rays, and harmonic contamination of the beam was prevented using a Rh-coated Si mirror. The intensities of the incident and transmitted X-rays were measured by the ion chamber detectors at room temperature.

The electrochemical behavior of $Li_zNi_{0.8}Co_{0.15}Al_{0.05}O_{2-\delta}$ was examined by using the sandwich-type electrochemical cell of Type TJ-AC (Tomcell Co. Ltd., Japan) with a lithium foil supported on a stainless steel plate as a negative electrode. The positive and negative electrodes separated by a microporous polypropylene film were immersed in 1 M $LiPF_6$ ethylene carbonate (EC)/dimethyl carbonate (DMC)/ethyl methyl carbonate (EMC) (3/4/3; volume ratio) electrolyte. 500 mAh-class cylindrical lithium-ion batteries consisting of wound sheets of $Li_zNi_{0.8}Co_{0.15}Al_{0.05}O_{2-\delta}$ positive-electrode and graphite negative-electrode with a microporous polypropylene film were also fabricated to examine the cycling stability at elevated temperature of 60˚C. Black viscous slurry of the positive electrode mix consisting of 85 wt% $Li_zNi_{0.8}Co_{0.15}Al_{0.05}O_{2-\delta}$, 10 wt% carbonblack, and 5 wt% polyvinylidene fluoride (PVdF) binder dissolved in N-methyl-2-pyrrolidone (NMP) was painted on one side of an aluminum foil for an electrochemical cell or on both sides for cylindrical lithium-ion batteries, and was dried under vacuum at 120˚C for 12 hours. The painted sheets were pressed to increase electrode density and cut to create positive electrodes. The graphite negative-electrodes were prepared in the same way as the positive electrodes, and consist of 95 wt% graphite and 5 wt% PVdF binder coated on copper foil.

The electrochemical cells were operated in a galvanostatic mode at C/10-rate in a voltage window of 4.2–2.5 V at 20˚C to examine the electrochemical reactivity of $Li_zNi_{0.8}Co_{0.15}Al_{0.05}O_{2-\delta}$. Intermittent charge and discharge measurement in a Galvanostatic Intermittent Titration Technique (GITT) mode of the electrochemical cells was performed at C/10-rate at 20˚C. The cell operation was interrupted every 10 mAh g^{-1}, and re-started when the voltage slope was below 1 mV h^{-1}.

The extended cycling test for cylindrical lithium-ion batteries of NCA-derivatives with graphite negative-electrode was performed for 500 cycles at elevated temperature of 60˚C in a voltage range of 4.1–3.0 V at 2C-rate.

3. Results and Discussion

3. 1 Preparation of $LiNi_{0.8}Co_{0.15}Al_{0.05}O_2$-derivatives Having Rock-salt Domains

In order to prepare NCA-derivatives having rock-salt domains, the ratios of lithium to metal ions in the starting materials were adjusted to be z = 1.05, 1.02, 1.00, 0.98, 0.95, 0.90, and 0.80 in $Li_zNi_{0.8}Co_{0.15}Al_{0.05}O_{2-\delta}$; X-ray diffraction (XRD) patterns of the obtained samples are displayed in **Fig. 5**. The chemical compositions of

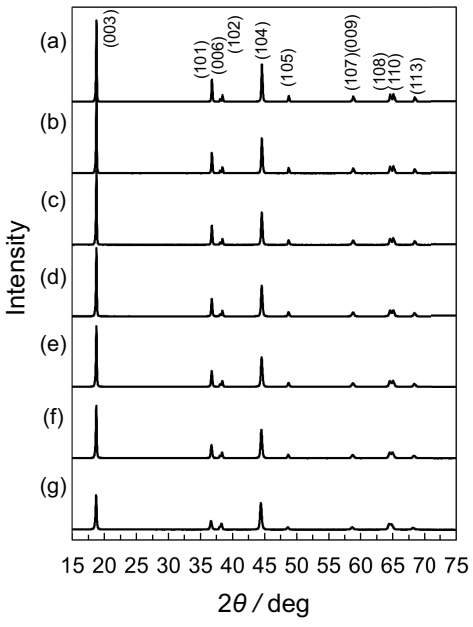

Fig. 5 XRD patterns of $Li_zNi_{0.8}Co_{0.15}Al_{0.05}O_{2-\delta}$ prepared by adjusting the Li/M ratios (M: $Ni_{0.8}Co_{0.15}Al_{0.05}$) of z = (a) 1.05, (b) 1.02, (c) 1.00, (d) 0.98, (e) 0.95, (f) 0.90, and (g) 0.80.

the samples were determined by inductively coupled plasma-atomic emission spectroscopy (ICP-AES), and are listed in **Table 2**. The lithium amounts listed in Table 2 are 2–3% less than the z-values, which is acceptable since these values can be explained by the 2–3% lithium evaporation during the heating process at 750°C in preparation. $Li_zNi_{0.8}Co_{0.15}Al_{0.05}O_{2-\delta}$ samples give the XRD patterns of the single phase associated with the rhombohedral lattice, and hence Miller indexes are given in hexagonal setting. Of these, $Li_zNi_{0.8}Co_{0.15}Al_{0.05}O_{2-\delta}$ (z = 1.05; NCA) shown in Fig. 5(a) exhibits a large diffraction peak of (003) in comparison to that of (104) and the clear peak-split of (006)/(102) or (108)/(110) in the XRD pattern, which indicates that $Li_zNi_{0.8}Co_{0.15}Al_{0.05}O_{2-\delta}$ (z = 1.05) has α-$NaFeO_2$-type layered structure. As z-value in $Li_zNi_{0.8}Co_{0.15}Al_{0.05}O_{2-\delta}$ decreases from 1.05 to 0.8, the (006) peak shifts to a higher diffraction angle toward the (102) peak, and the (110) peak approaches the (108) peak in its location. The (003) peak intensity decreases while that of (104) keeps constant value. Such changes in the peak intensity and location are ascribed to increased transition metal ions especially nickel ions at the lithium layers in α-$NaFeO_2$-type layered structure.[7,37] In NCA-derivatives prepared in this work, the rock-salt domains should be uniformly distributed in the lithium layers. Scanning transmission electron microscopy (STEM) will give us more insight into the distribution of nickel ions in the lithium layers as has been reported in our previous papers.[38,39] Such an approach is in progress in our research group. Rietveld analyses of the XRD patterns of $Li_zNi_{0.8}Co_{0.15}Al_{0.05}O_{2-\delta}$ ($0.8 \leq z \leq 1.05$) samples were performed by assuming the structural model of $[Li_{1-y}Ni_y]^{3(b)}[Ni,Co,Al]^{3(a)}O_2^{6(c)}$ based on a space group of $R\bar{3}m$. The Rietveld analytical results on the sample of z = 0.90 are shown in **Fig. 6** and the analytical results on those of $0.8 \leq z \leq 1.05$ are summarized in **Table 3**. Oxygen positional parameters of Zox are 0.2591–0.2598, which are consistent with previous results.[6,40,41] The y-value is estimated to be 0.0023 at z = 1.05, and increases to 0.1280 at z = 0.8. The values of (1−y)/(1+y) were calculated to confirm the validity of the analysis and should be comparable to the z-value in $Li_zNi_{0.8}Co_{0.15}Al_{0.05}O_{2-\delta}$. As listed in Table 3, the (1−y)/(1+y) values are 2–3% less than the z-values, which is comparable to the analytical results by ICP-AES listed in Table 2. The y-values of the samples of z = 1.05 and 1.02 are positive numbers in spite of the lithium-excess amount of z > 1.0 in preparation of the samples, which indicates that $LiNiO_2$-based materials do not have lithium ions in transition metal layers as reported by Delmas's research group.[7,41] Such a phenomenon does not occur in the case of $Li(Ni,Co,Mn)O_2$ positive-electrode materials since layered lithium manganese oxides can accommodate lithium ions in transition metal layers like Li_2MnO_3 (or $Li[Li_{1/3}Mn_{2/3}]O_2$ in layered formulation).[42-44] The hexagonal cell parameters, a and c, increase and the c/a ratio decreases as the y-value increases, as recorded in Table 1. The c/a ratio of the cubic symmetry should be about 4.899, and hence the change in c/a ratios from 4.95 to 4.94 indicates the change in symmetry

Table 2 Summary on the compositions of the samples, $Li_zNi_{0.8}Co_{0.15}Al_{0.05}O_{2-\delta}$ (z = 0.8–1.05), determined by inductively coupled plasma-atomic emission spectroscopy (ICP-AES).

z	Compositions [Liz(Ni,Co,Al)]			
	Li	Ni	Co	Al
1.05	1.042	0.810	0.144	0.046
1.02	1.002	0.809	0.145	0.046
1.00	0.989	0.810	0.144	0.046
0.98	0.960	0.811	0.144	0.046
0.95	0.938	0.810	0.144	0.046
0.9	0.886	0.810	0.144	0.046
0.8	0.787	0.809	0.145	0.047

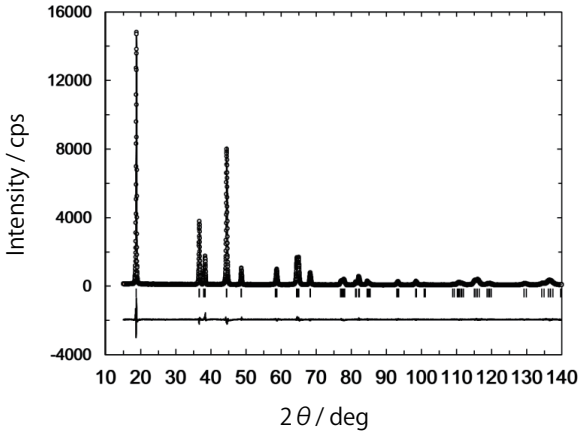

Fig. 6 Rietveld analytical result on $LizNi_{0.8}Co_{0.15}Al_{0.05}O_{2-\delta}$ (z = 0.90) assuming a space group of $R\bar{3}m$. Open circles indicate observed intensity and a solid curve indicates the calculated pattern by using parameters listed in Table I. Difference between observed and calculated patterns is shown at the bottom.

Table 3 Summary on the Rietveld analysis of $Li_zNi_{0.8}Co_{0.15}Al_{0.05}O_{2-\delta}$ (z = 0.8–1.05) showing the structure to be of $[Li_{1-y}Ni_y]^{3(b)}[Ni,Co,Al]^{3(a)}O_2$ based on a space group of $R\bar{3}m$.

z	Refined Structure	(1-y)/(1+y)	Lattice a-axis	Lattice c-axis	c/a	Zox	wRp	Rp
1.05	$[Li_{0.9977}Ni_{0.0023}]^{3(b)}[Ni_{0.7995}Co_{0.1503}Al_{0.0501}]^{3(a)}O_2$	0.995	2.864	14.180	4.951	0.2596	11.60	8.22
1.02	$[Li_{0.9948}Ni_{0.0052}]^{3(b)}[Ni_{0.7990}Co_{0.1508}Al_{0.0503}]^{3(a)}O_2$	0.990	2.864	14.182	4.952	0.2598	11.34	8.06
1.00	$[Li_{0.9907}Ni_{0.0093}]^{3(b)}[Ni_{0.7981}Co_{0.1514}Al_{0.0505}]^{3(a)}O_2$	0.982	2.865	14.185	4.951	0.2598	10.84	7.77
0.98	$[Li_{0.9806}Ni_{0.0194}]^{3(b)}[Ni_{0.7961}Co_{0.1529}Al_{0.0510}]^{3(a)}O_2$	0.962	2.866	14.187	4.950	0.2595	10.60	7.64
0.95	$[Li_{0.9627}Ni_{0.0373}]^{3(b)}[Ni_{0.7925}Co_{0.1556}Al_{0.0519}]^{3(a)}O_2$	0.928	2.867	14.191	4.950	0.2596	10.42	7.63
0.9	$[Li_{0.9393}Ni_{0.0607}]^{3(b)}[Ni_{0.7879}Co_{0.1591}Al_{0.0530}]^{3(a)}O_2$	0.886	2.870	14.197	4.947	0.2594	9.75	7.17
0.8	$[Li_{0.8720}Ni_{0.1280}]^{3(b)}[Ni_{0.7744}Co_{0.1692}Al_{0.0564}]^{3(a)}O_2$	0.773	2.876	14.214	4.942	0.2590	8.32	6.38

from rhombohedral toward cubic lattice. The a-axis parameter is the edge distance of unit octahedron MO_6 (M: Ni, Co, Al), which reflects the change in bond length of M–O, since the combination of MO_6 octahedra gives a two-dimensional layer forming the triangular lattice of sites.[12] The increase in the a-axis parameter indicates that the M–O bond length increases, which is ascribed to the reduction of transition metal ions.[37] In order to examine the oxidation states of nickel and cobalt ions in NCA-derivatives, XAFS measurements were conducted; the Ni K-edge X-ray absorption near-edge structure (XANES) spectra are displayed in **Fig. 7**. The oxidation state of cobalt ion in NCA-derivatives is invariable with respect to y-value according to the Co K-edge XANES spectra (not shown), which indicates that cobalt ions keep Co^{3+} in the oxidation state. As displayed in Fig. 7(a), a monotonous Ni K-edge shift to lower energy is seen as the y-value increases, indicating a reduction of nickel ions in NCA-derivatives. Edge energies at half-step height are displayed in Fig. 7(b), which are the energies at normalized absorbance of 0.5 and are often used to estimate the oxidation state of nickel ions.[45] The NCA sample of y = 0.0023 was prepared by lithium-excess amount z > 1, and therefore the oxidation state of nickel ion is close to Ni^{3+}. The edge energy follows a descending line, which indicates that NCA-derivatives having rock-salt domains are actually prepared to examine the cycling test of sandwich-type lithium cells and cylindrical lithium-ion batteries.

As described above, NCA-derivatives of $Li_zNi_{0.8}Co_{0.15}Al_{0.05}O_{2-\delta}$ ($0.8 \leq z \leq 1.05$) were prepared and refined by a Rietveld method of the XRD patterns to be $[Li_{1-y}Ni_y]^{3(b)}[Ni,Co,Al]^{3(a)}O_2$[6(c)]

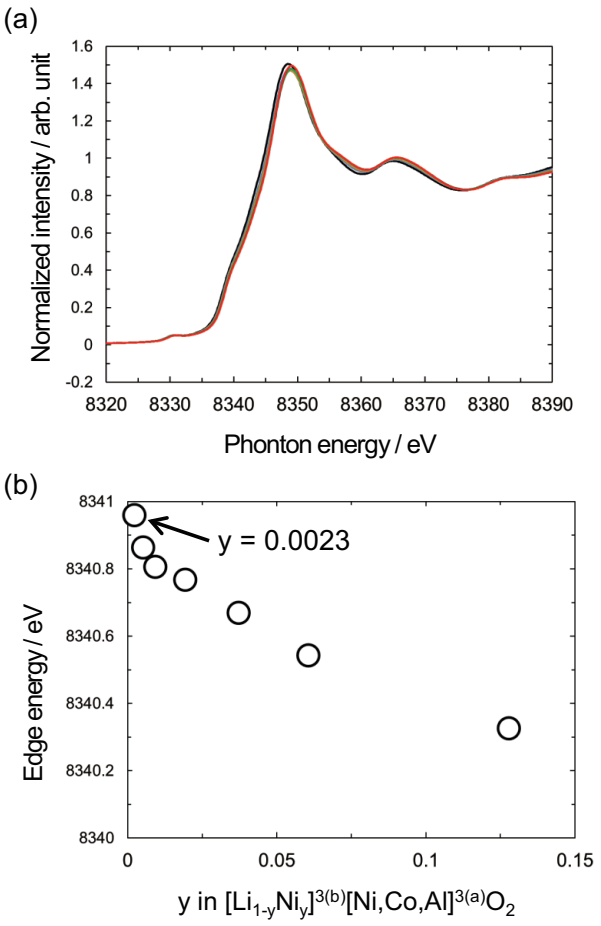

Fig. 7 (a) Ni K-edge XANES spectra of $LizNi_{0.8}Co_{0.15}Al_{0.05}O_{2-\delta}$ corresponding to $[Li_{1-y}Ni_y]^{3(b)}[Ni,Co,Al]^{3(a)}O_2$ based on a space group of $R\bar{3}m$ at room temperature. Edge energies at half-step heights as a function of amount of rock-salt domains, y, are also displayed in (b).

($0.0023 \leq y \leq 0.1280$) based on a space group of $R\bar{3}m$. Nickel ions are reduced from the oxidation state of Ni^{3+} toward Ni^{2+} in the layered structure as the y-value increases. Nickel ions of Ni^{2+} in the oxidation states are incorporated into the lithium layers because of the similarity of the ionic radii between Li^{+} and Ni^{2+} ions.[7,41,46] These results indicate that the y-values are the amounts of rock-salt domains in NCA-derivatives and the rock-salt domains correspond to the degradation of the positive electrode that appeared during the extended cycling test of cylindrical lithium-ion batteries at elevated temperature above 60°C.[28,29] The amounts of rock-salt domains in NCA-derivative prepared in this work were as high as 12.8%, and can be quantitatively controlled within 0.23–12.8%. These NCA-derivatives were applied to examine electrochemical reactivity in sandwich-type lithium cells and the extended cycling test at 60°C of cylindrical lithium-ion batteries with graphite-negative electrode.

2. Rechargeable Capacities of $LiNi_{0.8}Co_{0.15}Al_{0.05}O_2$- derivatives

In order to examine the electrochemical reactivity of NCA-derivatives having rock-salt domains in terms of a voltage profile in sandwich-type lithium cells, constant-current charge and discharge measurement was performed at C/10-rate in a voltage window of 4.2–2.5 V at 20°C. **Figure 8** displays the voltage profiles of sandwich-type lithium cells of NCA-derivatives. The sandwich-type lithium cell of NCA (y = 0.0023) exhibits an ascending curve from 3.6 to 4.2 V on charge and then the discharge curve just traces the charge one in the reverse direction. The first charge and discharge capacities were 205 and 177 mAh g^{-1}, respectively, which means that a capacity of 28 mAh g^{-1} was lost during the first cycle, i.e., so-called irreversible capacity. As the amount of rock-salt domains in NCA-derivatives increases, rechargeable capacity decreases from 177 mAh g^{-1} at y = 0.0023 to about 90 mAh g^{-1} at y = 0.1280, which corresponds to capacity fading owing to increased rock-salt domains. **Figure 9** shows rechargeable capacity as a function of y-value in $[Li_{1-y}Ni_y]^{3(b)}[Ni,Co,Al]^{3(a)}O_2{}^{6(c)}$ ($0.0023 \leq y \leq 0.1280$) based on the space group of $R\bar{3}m$. The dotted line of the rechargeable capacity was drawn in the figure by assuming that the nickel ions in lithium layers are inactive. Although a linear relation between rechargeable capacities (Q) and y-value is actually seen in the figure, the obtained rechargeable capacities are below the dotted line. The empirical equation is obtained as $Q = 181.4 - 725.5\ y$, in which Q reaches zero at $y \approx 0.25$, indicating that rechargeable capacity is completely lost when the nickel ions at the lithium layers increase to about 25% of NCA, which cannot be explained simply by the capacity-loss derived from the increased inactive rock-salt domain in the structure. As shown in Fig. 8, decreased rechargeable capacities are associated with small first-charge capacities and large irreversible capacities in the first cycle, and those are ascribed to not only the capacity-loss derived from

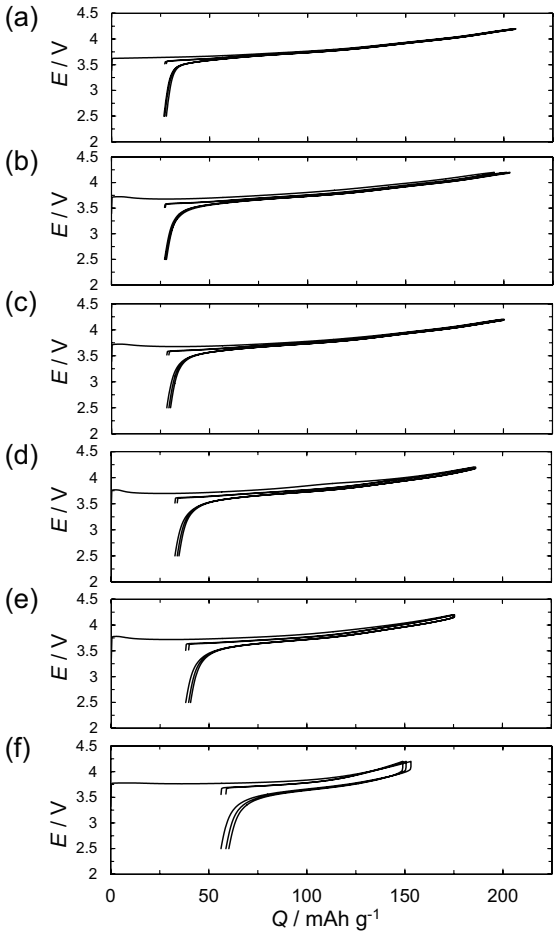

Fig. 8 Voltage profiles of sandwich-type lithium cells of $LizNi_{0.8}Co_{0.15}Al_{0.05}O_{2-\delta}$ corresponding to $[Li_{1-y}Ni_y]^{3(b)}[Ni,Co,Al]^{3(a)}O_2$ based on a space group of $R\bar{3}m$; y [z] = (a) 0.0023 [1.05], (b) 0.0093 [1.00], (c) 0.0194 [0.98], (d) 0.0373 [0.95], (e) 0.0607 [0.90], and (f) 0.1280 [0.80]. The cells were operated in a voltage window of 4.2–2.5 V at C/10-rate at 20°C.

inactive rock-salt domain but the polarization-increase, which is shown in voltage profiles as the large difference in operating voltage between charge and discharge operations.

3. 3 Change in Polarizations of $LiNi_{0.8}Co_{0.15}Al_{0.05}O_2$- derivatives during Charge and Discharge

Lithium-ion mobility in the bulk structure rather than the reaction at the interface was examined by the intermittent charge and discharge measurement of sandwich-type lithium cells of NCA-derivatives in a Galvanostatic Intermittent Titration Technique (GITT) mode.[47-49] **Figure 10** displays voltage profiles of NCA-derivatives for y = 0.0023, 0.0607, and 0.1280, and their polarizations defined as a difference in voltage after the lapse of 2 sec to the end of the relaxation period, which is associated with mass transfer since ohmic and charge-transfer resistances appear in a short time within 2 sec. As shown in Fig. 10(a), polarizations of NCA (y = 0.0023) are quite small, 2.3–3.4 mV, on both charge and discharge over an entire range of the cell operation. Increased polarizations are seen at low-voltage region of about 3.5–3.6 V on both charge and discharge. An NCA-derivative with increased rock-salt domains (y = 0.0607) shown in Fig. 10(b) exhibits larger polarization than NCA (y = 0.0023) especially at the end of charge or discharge, producing U-shaped curves of polarizations. Such degradation in electrochemical reactivity producing U-shaped curves

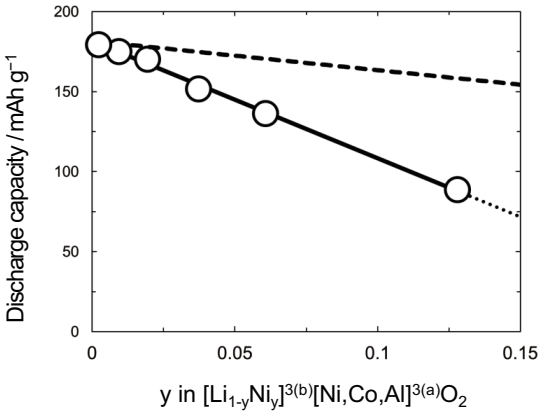

Fig. 9 Discharge capacities as a function of y in $[Li_{1-y}Ni_y]^{3(b)}[Ni,Co,Al]^{3(a)}O_2$ based on a space group of $R\bar{3}m$ at 20°C. A dotted line was drawn by assuming that the nickel ions in lithium layers were inactive.

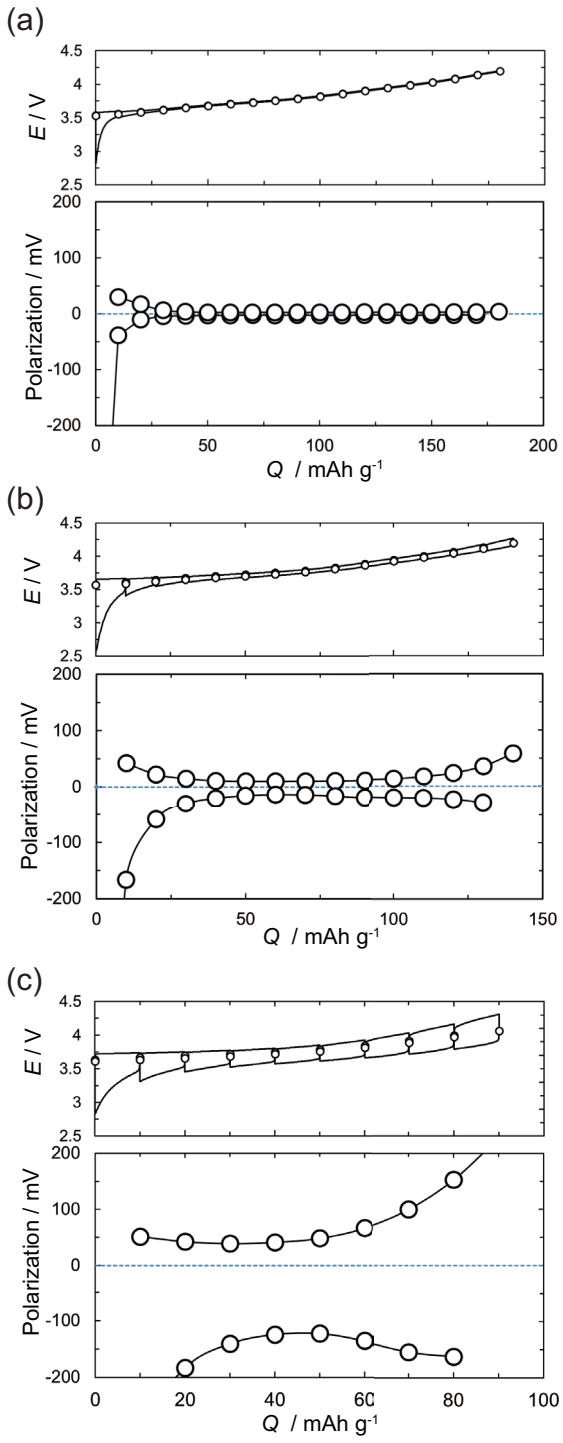

Fig. 10 Intermittent charge and discharge curves in a GITT mode of sandwich-type lithium cells of $[Li^{1-y}Ni_y]^{3(b)}[Ni,Co,Al]^{3(a)}O_2$ of y = (a) 0.0023, (b) 0.0607, and (c) 0.1280 at C/10-rate at 20°C. The cell operation was interrupted every 10 mAh g^{-1}, and re-started when the voltage slope was below 1 mV h^{-1}. Polarizations defined as a difference in voltage after the lapse of 2 sec to the end of the relaxation period are also displayed. Polarizations on charge are given as positive numbers and those on discharge are given as negative numbers.

of polarization is quite obvious in the NCA-derivative having the largest amount of rock-salt domains (y = 0.1280). Figure 10(c) (y = 0.1280) clearly shows increased polarization at the end of charge or discharge, and polarizations on discharge are larger than those on charge over the entire range of cell operation. At the end of charge, increased polarization is one of the reasons for the decrease in rechargeable capacity as a function of amount of rock-salt domains, and at the end of discharge, large polarization is characteristic of the appearance of the irreversible capacity seen in the first cycle.

In order to examine the electrochemical reactivity in the irreversible region, intermittent charge and discharge operation of NCA (y = 0.0023) was continued through the irreversible region; the voltage profile is shown in **Fig. 11**. The open-circuit voltages on discharge in the irreversible region are the same as those on charge, and the cell can be discharged back to the initial 0 mAh g^{-1}, which indicates that the irreversible capacity in the first cycle can be recovered by an intermittent mode. **Figure 12** displays the voltage profiles of NCA (y = 0.0023) operated in a 200 mAh g^{-1} capacity-limited mode at 20, 60, and 80°C. Although NCA exhibits 25 mAh g^{-1} of irreversible capacity at 20°C, this can be recovered with low-voltage discharge below 2.0 V. As shown in Fig. 12, the so-called irreversible capacity shrinks from 25 mAh g^{-1} at 20°C to below 10 mAh g^{-1} at elevated temperature. These results indicate that the irreversible capacity is under kinetic control. **Figure 13** displays the crystal structure of an NCA-derivative having rock-salt domains. The mechanisms of the irreversible capacity have been proposed by several research groups, and have been discussed from the viewpoint of lithium-ion mobility in the crystal structure. Delmas et al. proposed an mechanism associated with Ni^{2+} ions placed in the lithium layers.[41] During the first charge, the Ni^{2+} ions in the lithium layers oxidize to smaller Ni^{3+} ions, which induce a local collapse in the structure. The local collapse makes it difficult to insert lithium ions back into the structure. Ceder et al. discussed lithium-ion mobility in terms of monovacancy or divacancy hopping associated with interlayer distance in the layered structure, and then Dahn et al. and Kang et al. discussed the irreversible capacity on the basis of results using Ceder's calculation.[50-53]

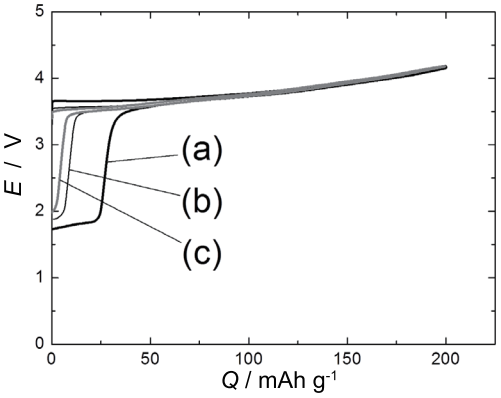

Fig. 12 Voltage profiles of sandwich-type lithium cell of $[Li_{1-y}Ni_y]^{3(b)}[Ni,Co,Al]^{3(a)}O_2$ of y = 0.0023 operated in a 200 mAh g^{-1} capacity-limited mode at C/10-rate at (a) 20, (b) 60, or (c) 80ºC.

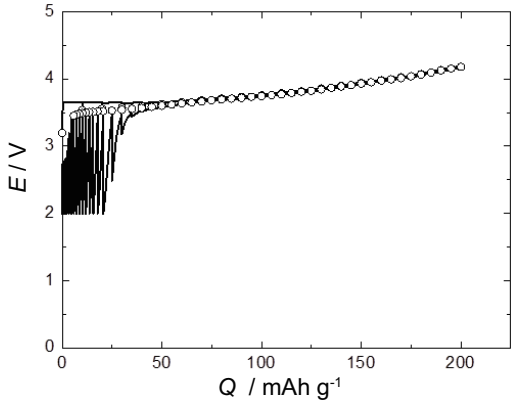

Fig. 11 Intermittent charge and discharge curve of sandwich-type lithium cell of $[Li_{1-y}Ni_y]^{3(b)}[Ni,Co,Al]^{3(a)}O_2$ of y = 0.0023 at C/10-rate at 20ºC.

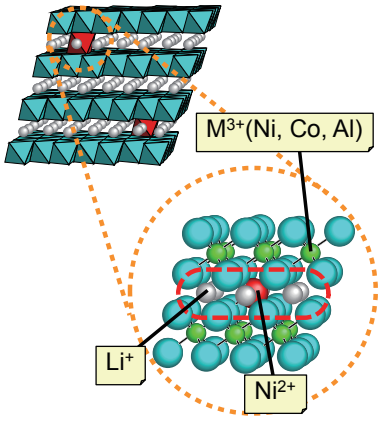

Fig. 13 Nickel ions at the lithium sheets in a layered structure of $[Li_{1-y}Ni_y]^{3(b)}[Ni,Co,Al]^{3(a)}O_2$ based on a space group of $R\bar{3}m$.

Our results on the irreversible capacity displayed in Figs. 11 and 12 strongly suggest that the irreversible capacity is derived from a kinetic limitation of lithium insertion into the structure. According to the relation between the increased irreversible capacity at the end of discharge and the polarization-increase over the entire range of operation, the increased polarizations of the NCA-derivatives having a large amount of rock-salt domains especially in the discharge direction or lithium-insertion direction into the structure are mainly derived from slow lithium-ion mobility owing to the nickel ions in the lithium layers.

Figure 14 shows polarizations of NCA-derivatives at the midpoint of the rechargeable capacity as a function of y-value in $[Li_{1-y}Ni_y]^{3(b)}[Ni,Co,Al]^{3(a)}O_2^{6(c)}$ based on the space group of $R\bar{3}m$. Polarizations of NCA-derivatives on discharge corresponding to lithium insertion into the structure are larger than those on charge. According to the results on the irreversible capacity, increased polarization of NCA-derivatives having rock-salt domains especially in the discharge direction is ascribed to slow lithium-ion mobility owing to the rock-salt domains. Polarizations increase when the amount of rock-salt domains is above 2%, i.e., $y > 0.02$, and the largest amount of rock-salt domains (12.8%) among the NCA-derivatives examined causes the largest polarizations: 41 mV on charge and 125 mV on discharge.

3. 4 Charge and Discharge Cycling Stability of $LiNi_{0.8}Co_{0.15}Al_{0.05}O_2$-derivatives

In order to examine the cumulative increase in polarization of the NCA-derivatives during charge and discharge cycles, a cycling test of sandwich-type lithium cells of the NCA-derivatives was performed at a low rate of C/10 at 20°C. This measurement is appropriate to examine materials degradation since the materials are exposed in a charged state to high voltages for almost a month and other factors of battery deterioration can be excluded. **Figure 15** displays the discharge capacities and capacity retentions of sandwich-type lithium cells of the NCA-derivatives. As shown in Fig. 15(a), discharge capacity decreases as amount of rock-salt domains increases. Of these, discharge capacities of the NCA-derivatives in $y < 0.02$ trace parallel lines during 30 cycles. This means that capacity retentions are almost the same values of 93–95% in 30 cycles for the samples having the rock-salt domains of below 2% as shown in Fig. 15(b). Capacity retention decreases to 69–70% when amount of rock-salt domains exceeds 2%. The NCA-derivative having the largest amount of rock-salt domains (12.8%) exhibits the lowest capacity retention for 30 cycles (58%) among the

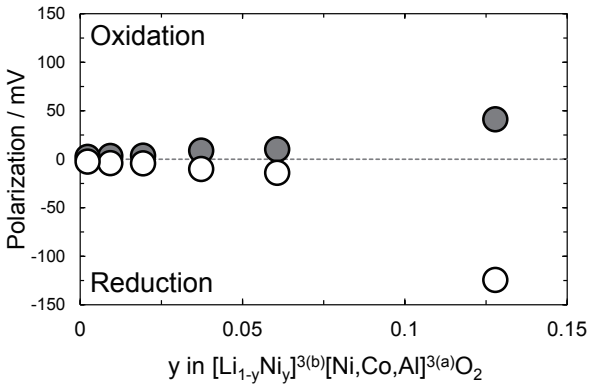

Fig. 14 Polarization at the midpoint of rechargeable capacity as a function of y in $[Li_{1-y}Ni_y]^{3(b)}[Ni,Co,Al]^{3(a)}O_2$ obtained by GITT experiments at C/10-rate at 20ºC.

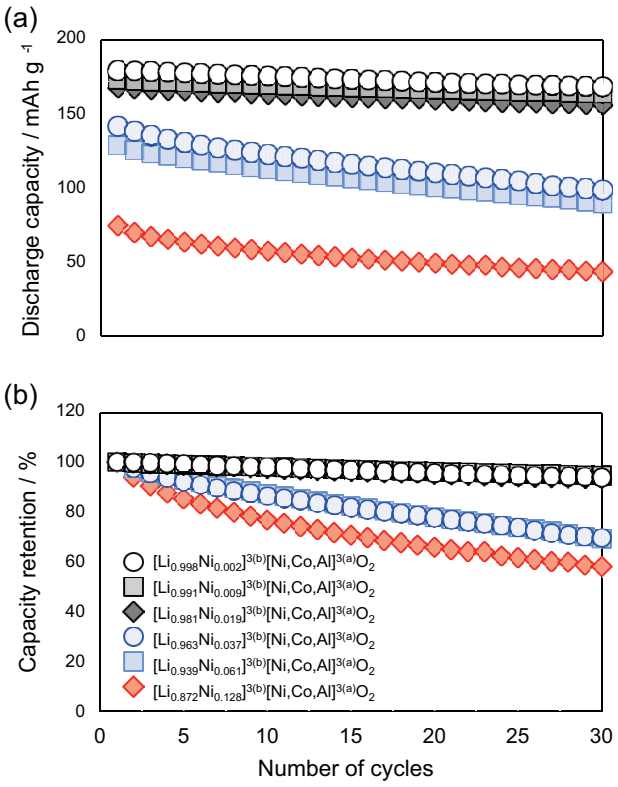

Fig. 15 (a) Discharge capacities and (b) capacity retentions for sandwich-type lithium cells of $[Li_{1-y}Ni_y]^{3(b)}[Ni,Co,Al]^{3(a)}O_2$ based on a space group of $R\bar{3}m$ operated in a voltage window of 4.2–2.5 V at C/10-rate at 20ºC.

NCA-derivatives. There seems to be a one-to-one correspondence between capacity retention for 30 cycles and amount of rock-salt domains in terms of the increased polarization examined by GITT measurement associated with the slow lithium-ion mobility derived from the rock-salt domains.

Such a polarization-increase during cycling is also superposed on the extended cycling test for cylindrical lithium-ion batteries at elevated temperature of 60°C. The NCA-derivatives of y = 0.0023 and 0.0607 were chosen to fabricate cylindrical lithium-ion batteries with graphite negative-electrode because they exhibited the characteristic capacity retentions in sandwich-type lithium cells for 30 cycles. The extended cycling test for cylindrical lithium-ion batteries were performed for 500 cycles at 2C-rate at elevated temperature of 60°C. **Figure 16** displays the capacity retentions of cylindrical lithium-ion batteries for 500 cycles. NCA of y = 0.0023 gives an 83% capacity retention in a cylindrical lithium-ion battery after 500 cycles at 60°C, and the capacity retention of the NCA-derivative of y = 0.0607 in a cylindrical battery is 73%, which is lower than that of NCA. Battery deterioration derived from materials degradation of NCA is accelerated when the NCA-derivatives have large amounts of rock-salt domains. Increased polarization during cycling owing to nickel ions at the lithium layers is the main factor affecting the accelerated deterioration of cycling life. These results on the NCA-derivatives strongly suggest that materials innovation to prevent the formation of rock-salt domains will improve the cycling life of cylindrical lithium-ion batteries at elevated temperature. Substitution of metal ions of lower oxidation states such as Mg^{2+} for nickel ions in NCA, which can act to increase the oxidation state of nickel ions, is one of the effective ways to improve battery performance.[18,27,35,54]

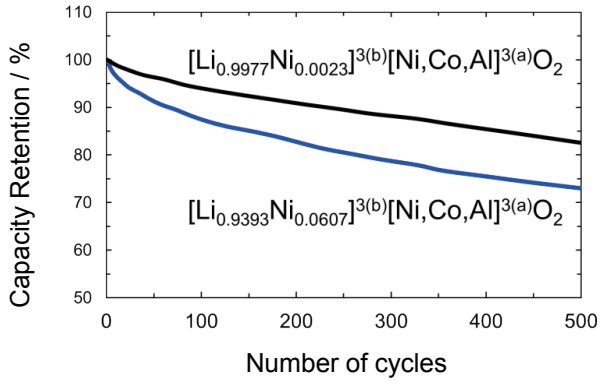

Fig. 16 Capacity retentions for 500 mAh-class cylindrical lithium-ion batteries of y = 0.0023 and 0.0607 in $[Li_{1-y}Ni_y]^{3(b)}[Ni,Co,Al]^{3(a)}O_2$ with graphite negative-electrode operated in a voltage window of 4.1–3.0 V at 2C-rate at 60°C.

4. Conclusion

In this paper, the way to describe crystal structure and the research background of positive electrode materials are presented. Cycling stability of lithium-ion batteries especially at elevated temperature above 60ºC has been reported to be mainly associated with electrochemical reactivity and structural stability of positive electrode materials such as $LiNi_{0.8}Co_{0.15}Al_{0.05}O_2$. NCA-derivatives of $Li_zNi_{0.8}Co_{0.15}Al_{0.05}O_{2-\delta}$ ($0.8 \leq z \leq 1.05$) or $[Li_{1-y}Ni_y]^{3(b)}[Ni,Co,Al]^{3(a)}O_2{}^{6(c)}$ based on a space group of $R\bar{3}m$, in which the y-value is the amount of rock-salt domains, were prepared by adjusting Li / (Ni, Co, Al) ratios and their electrochemical measurements in sandwich-type lithium cells were performed to clarify the relation between the amount of rock-salt domains and electrochemical reactivity in terms of rechargeable capacity and polarization. Rechargeable capacities of NCA-derivatives in sandwich-type lithium cells decrease linearly as a function of y-value and reach zero at $y \approx 0.25$ according to extrapolating by a straight line. Such a relation is derived from not only the lost capacity owing to inactive rock-salt domains but the increased polarization. GITT measurement told us that nickel ions at the lithium layers in NCA of above 2% cause polarization-increase especially during discharge operation or lithium insertion into the structure, which is ascribed to slow lithium-ion mobility owing to nickel ions in the lithium layers. Low-rate cycling test of sandwich-type lithium cells of NCA-derivatives indicated that the accelerated capacity-fading is associated with the increased polarization. Extended cycling test of cylindrical lithium-ion batteries with graphite negative-electrode at elevated temperature of 60°C indicated that rock-salt domains in NCA cause and accelerate further degradation. Materials innovation to prevent the formation of rock-salt domains will be an effective way to improve the cycling life of lithium-ion batteries at elevated temperature.

Cation-doping and substitution based on the formation of solid solution have been performed to

improve electrochemical reactivity and structural stability of positive electrode materials. In order to stabilize the layered structure of $LiNiO_2$ and to enhance the electrochemical reactivity, metal ions of Mg^{2+}, Al^{3+}, Co^{3+}, Fe^{3+} ions, etc., were doped in $LiNiO_2$. Of these, Mg^{2+} ions can be substituted for nickel ions in $LiNiO_2$ or NCA. Substitution of Mg^{2+} ions in NCA is an effective way to improve the capacity-fading and the increase in internal resistance of lithium-ion batteries. These approaches have been reported in the research papers and listed in the references below.[18, 27, 35, 54]

References

(1) Whittingham, M. S., *Chem. Rev.*, Vol. 104, No. 10 (2004), pp. 4271-4301.
(2) Ohzuku, T. and Brodd, R. J., *J. Power Sources*, Vol. 174, No. 2 (2007), pp. 449-456.
(3) Ellis, B. L., Lee, K. T. and Nazar, L. F., *Chem. Mater.*, Vol. 22, No. 3 (2010), pp. 691-714.
(4) Etacheri, V., Marom, R., Elazari, R., Salitra, G. and Aurbach, D., *Energy Environ. Sci.*, Vol. 4, No. 9 (2011), pp. 3243-3262.
(5) Mizushima, K., Jones, P. C., Wiseman, P. J. and Goodenough, J. B., *Mat. Res. Bull.*, Vol. 15, No. 6 (1980), pp. 783-789.
(6) Ohzuku, T., Ueda, A. and Nagayama, M., *J. Electrochem. Soc.*, Vol. 140, No. 7 (1993), pp. 1862-1870.
(7) Delmas, C., Ménétrier M., Croguennec, L., Saadoune, I., Rougier, A., Pouillerie, C., Prado, G., Grüne, M. and Fournès, L., *Electrochim. Acta*, Vol. 45, No. 1-2 (1999), pp. 243-253.
(8) Boulineau, A., Croguennec, L., Delmas, C. and Weill, F., *Solid State Ionics*, Vol. 180, No. 40 (2010), pp. 1652-1659.
(9) Delmas, C., Braconnier, J.-J., Maazaz, A. and Hagenmuller, P., *Rev. Chim. Miner.*, Vol. 19 (1982) 343.
(10) Paulsen, J. M., Thomas, C. L. and Dahn, J. R., *J. Electrochem. Soc.*, Vol. 146, No. 10 (1999), pp. 3560-3565.
(11) Paulsen, J. M., Donaberger, R. A. and Dahn, J. R., *Chem. Mater.*, Vol. 12, No. 8 (2000), pp. 2257-2267.
(12) Ohzuku, T. and Makimura, Y., *Res. Chem. Intermed.*, Vol. 32, No. 5 (2006), pp. 507-521.
(13) Ohzuku, T. and Ueda, A., *J. Electrochem. Soc.*, Vol. 144, No. 8 (1997), pp. 2780-2785.
(14) Ohzuku, T., Ueda, A. and Kouguchi, M., *J. Electrochem. Soc.*, Vol. 142, No. 12 (1995), pp. 4033-4039.
(15) Tobishima, S. and Yamaki, J., *J. Power Sources*, Vol. 81-82 (1999), pp. 882-886.
(16) Leising, R. A., Palazzo, M. J., Takeuchi, E. S. and Takeuchi, K. J., *J. Electrochem. Soc.*, Vol. 148, No. 8 (2001), pp. A838-A844.
(17) Ohsaki, T., Kishi, T., Kuboki, T., Takami, N., Shimura, N., Sato, Y., Sekino, M. and Satoh, A., *J. Power Sources*, Vol. 146, No. 1-2 (2005), pp. 97-100.
(18) Sasaki, T., Godbole, V., Takeuchi, Y., Ukyo, Y. and Novák, P., *J. Electrochem. Soc.*, Vol. 158, No. 11 (2011), pp. A1214-A1219.
(19) Watanabe, S., Kinoshita, M., Hosokawa, T., Morigaki, K. and Nakura, K., *J. Power Sources*, Vol. 258 (2014), pp. 210-217.
(20) Watanabe, S., Kinoshita, M., Hosokawa, T., Morigaki, K. and Nakura, K., *J. Power Sources*, Vol. 260 (2014), pp. 50-56.
(21) Amine, K., Chen, C. H., Liu, J., Hammond, M., Jansen, A., Dees, D., Bloom, I., Vissers, D. and Henriksen, G., *J. Power Sources*, Vol. 97-98 (2001), pp. 684-687.
(22) Shim, J., Kostecki, R., Richardson, T., Song, X. and Striebel, K. A., *J. Power Sources*, Vol. 112, No. 1 (2002), pp. 222-230.
(23) Abraham, D. P., Twesten, R. D., Balasubramanian, M., Petrov, I., McBreen, J. and Amine, K., *Electrochem. Commun.*, Vol. 4, No. 8 (2002), pp. 620-625.
(24) Abraham, D. P., Twesten, R. D., Balasubramanian, M., Kropf J., Fischer, D., McBreen, J., Petrov, I. and Anine, K., *J. Electrochem. Soc.*, Vol. 150, No. 11 (2003), pp. A1450-A1456.
(25) Itou, Y. and Ukyo, Y., *J. Power Sources*, Vol. 146, No. 1-2 (2005), pp. 39-44.
(26) Kostecki, R., Lei, J., McLarnon, F., Shim, J. and Striebel, K., *J. Electrochem. Soc.*, Vol. 153, No. 4 (2006), pp. A669-A672.
(27) Kondo, H., Takeuchi, Y., Sasaki, T., Kawauchi, S., Itou, Y., Hiruta, O., Okuda, C., Yonemura, M., Kamiyama, T. and Ukyo, Y., *J. Power Sources*, Vol. 174, No. 2 (2007), pp. 1131-1136.
(28) Sasaki, T., Nonaka, T., Oka, H., Okuda, C., Itou, Y., Kondo, Y., Takeuchi, Y., Ukyo, Y., Tatsumi, K. and Muto, S., *J. Electrochem. Soc.*, Vol. 156, No. 4 (2009), pp. A289-A293.
(29) Muto, S., Sasano, Y., Tatsumi, K., Sasaki, T., Horibuchi, K., Takeuchi, Y. and Ukyo, Y., *J. Electrochem. Soc.*, Vol. 156, No. 5 (2009), pp. A371-A377.
(30) Hayashi, T., Okada, J., Toda, E., Kuzuo, R., Oshimura, N., Kuwata, N. and Kawamura, J., *J. Electrochem. Soc.*, Vol. 161, No. 6 (2014), pp. A1007-A1011.
(31) Makimura, Y., Okuda, C., Nonaka, T., Nishimura, Y. F., Sasaki, T. and Takeuchi, Y., *ECS Electrochem. Lett.*, Vol. 3, No. 6 (2014), pp. A66-A68.
(32) Guilmard, M., Croguennec, L., Denux, D. and Delmas, C., *Chem. Mater.*, Vol. 15, No. 23 (2003), pp. 4476-4483.

(33) Guilmard, M., Croguennec, L. and Delmas, C., *Chem. Mater.*, Vol. 15, No. 23 (2003), pp. 4484-4493.
(34) Bang, H.-J., Joachin, H., Yang, H., Amine, K. and Prakash, J., *J. Electrochem. Soc.*, Vol. 153, No. 4 (2006), pp. A731-737.
(35) Muto, S., Tatsumi, K., Kojima, Y., Oka, H., Kondo, H., Horibuchi, K. and Ukyo, Y., *J. Power Sources*, Vol. 205 (2012), pp. 449-455.
(36) Toby, B. H., *J. Appl. Crystallogr.*, Vol. 34, No. 2 (2001), pp. 210-213.
(37) Rougier, A., Gravereau, P. and Delmas, C., *J. Electrochem. Soc.*, Vol. 143, No. 4 (1996), pp. 1168-1175.
(38) Zheng, S., Huang, R., Makimura, Y., Ukyo, Y., Fisher, C. A. J., Hirayama, T. and Ikuhara, Y., *J. Electrochem. Soc.*, Vol. 158, No. 4 (2011), pp. A357-A362.
(39) Makimura, Y., Zheng, S., Ikuhara, Y. and Ukyo, Y., *J. Electrochem. Soc.*, Vol. 159, No. 7 (2012), pp. A1070-A1073.
(40) Ohzuku, T., Ueda, A., Nagayama, M., Iwakoshi, Y. and Komori, H., *Electrochim. Acta*, Vol. 38, No. 9 (1993), pp. 1159-1167.
(41) Delmas, C., Pérès, J. P., Rougier, A., Demourgues, A., Weill, F., Chadwick, A., Broussely, M., Perton, F., Biensan, P. and Willmann, P., *J. Power Sources*, Vol. 68, No. 1 (1997), pp. 120-125.
(42) Ammundsen, B. and Paulsen, J., *Adv. Mater.*, Vol. 13, No. 12-13 (2001), pp. 943-956.
(43) Ohzuku, T., Ariyoshi, K., Makimura, Y., Yabuuchi, N. and Sawai, K., *Electrochemistry*, Vol. 73 (2005), pp. 2-11.
(44) Thackeray, M. M., Kang, S.-H., Johnson, C. S., Vaughey, J. T., Benedek, R. and Hackney, S. A., *J. Mater. Chem.*, Vol. 17, No. 30 (2007), pp. 3112-3125.
(45) Mansour, A. N. and Melendres, C. A., *J. Phys. Chem. A*, Vol. 102, No. 1 (1998), pp. 65-81.
(46) Shannon, R. D., *Acta Cryst.*, Vol. A32 (1976), pp. 751-767.
(47) Weppner, W. and Huggins, R. A., *J. Electrochem. Soc.*, Vol. 124, No. 10 (1977), pp. 1569-1578.
(48) Dees, D. W., Kawauchi, S., Abraham, D. P. and Prakash, J., *J. Power Sources*, Vol. 189, No. 1 (2009), pp. 263-268.
(49) Amin, R., Ravnsbæk, D. B. and Chiang, Y.-M., *J. Electrochem. Soc.*, Vol. 162, No. 7 (2015), pp. A1163-A1169.
(50) Van der Ven, A. and Ceder, G., *Electrochemical Solid-State Lett.*, Vol. 3, No. 7 (2000), pp. 301-304.
(51) Mueller-Neuhaus, J. R., Dunlap, R. A. and Dahn, J. R., *J. Electrochem. Soc.*, Vol. 147, No. 10 (2000), pp. 3598-3605.
(52) Van der Ven, A. and Ceder, G., *J. Power Sources*, Vol. 97-98 (2001), pp. 529-531.
(53) Kang, K. and Ceder, G., *Phys. Rev. B*, Vol. 74, No. 9 (2006), 094105.
(54) Tatsumi, K., Sasano, Y., Muto, S., Yoshida, T., Sasaki, T., Horibuchi, K., Takeuchi, Y. and Ukyo, Y., *Phys. Rev. B*, Vol. 78, No. 4 (2008), 045108.

Yoshinari Makimura
Research Fields:
- Solid-State Chemistry
- Electrochemistry of Inorganic Compounds for Energy Storage Devices

Academic Degree: Ph.D.
Academic Societies:
- The Electrochemical Society of Japan
- The Electrochemical Society

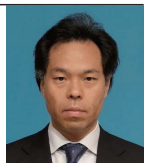

Tsuyoshi Sasaki
Research Fields:
- Batteries and Battery Materials
- Electrochemistry

Academic Degree: Dr.Eng.
Academic Societies:
- The Electrochemical Society
- International Society of Electrochemistry
- The Ceramic Society of Japan
- The Japan Institute of Metals and Materials
- The Electrochemical Society of Japan

Takamasa Nonaka
Research Field:
- Materials Analysis Using Synchrotron Radiation

Academic Degree: Dr.Eng.
Academic Society:
- The Japanese Society for Synchrotron Radiation Research

Award:
- Promotion Award from the Ceramic Society of Japan (2008)